NANO LETTERS

Letter

pubs.acs.org/NanoLett

Stable Graphene-Two-Dimensional Multiphase Perovskite Heterostructure Phototransistors with High Gain

Yuchuan Shao,[†] Ye Liu,[‡] Xiaolong Chen,[†] Chen Chen,[†] Ibrahim Sarpkaya,[†,⊥] Zhaolai Chen,[‡] Yanjun Fang,[‡] Jaemin Kong,[§] Kenji Watanabe,[∥] Takashi Taniguchi,[∥] André Taylor,[§] Jinsong Huang,*[,‡] and Fengnian Xia*[,†]

[†]Department of Electrical Engineering, Yale University, 15 Prospect Street Becton 519, New Haven, Connecticut 06511, United States

[‡]Department of Mechanical and Materials Engineering and Nebraska Center for Materials and Nanoscience, University of Nebraska-Lincoln, Lincoln, Nebraska 68588-0656, United States

[§]Department of Chemical and Environmental Engineering, Yale University, 9 Hillhouse Avenue, New Haven, Connecticut 06511, United States

[∥]Advanced Materials Laboratory, National Institute for Materials Science, 1-1 Namiki, Tsukuba 305-0044, Japan

S *Supporting Information*

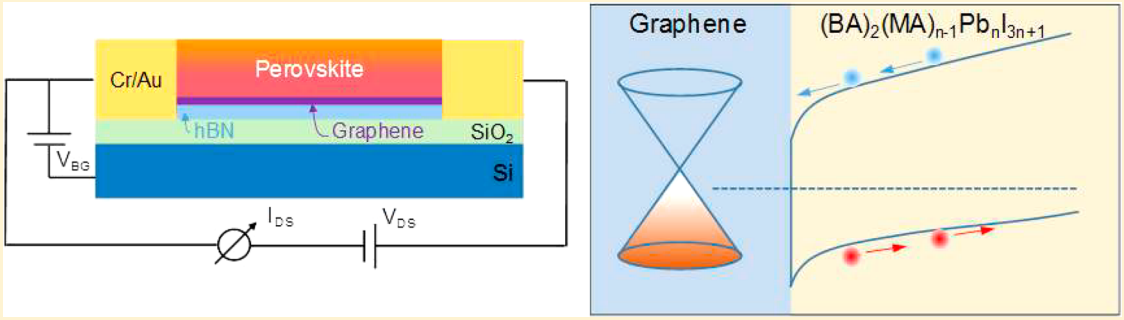

ABSTRACT: Recently, two-dimensional (2D) organic−inorganic perovskites emerged as an alternative material for their three-dimensional (3D) counterparts in photovoltaic applications with improved moisture resistance. Here, we report a stable, high-gain phototransistor consisting of a monolayer graphene on hexagonal boron nitride (hBN) covered by a 2D multiphase perovskite heterostructure, which was realized using a newly developed two-step ligand exchange method. In this phototransistor, the multiple phases with varying bandgap in 2D perovskite thin films are aligned for the efficient electron−hole pair separation, leading to a high responsivity of $\sim 10^5$ A W^{-1} at 532 nm. Moreover, the designed phase alignment method aggregates more hydrophobic butylammonium cations close to the upper surface of the 2D perovskite thin film, preventing the permeation of moisture and enhancing the device stability dramatically. In addition, faster photoresponse and smaller $1/f$ noise observed in the 2D perovskite phototransistors indicate a smaller density of deep hole traps in the 2D perovskite thin film compared with their 3D counterparts. These desirable properties not only improve the performance of the phototransistor, but also provide a new direction for the future enhancement of the efficiency of 2D perovskite photovoltaics.

KEYWORDS: *Two-dimensional perovskite, graphene, phototransistors, photoconductive gain, stability*

Graphene photodetectors exhibit many desirable properties such as high speed arising from its high mobility,[1] broadband absorption,[2] and their ease in its integration with other waveguide systems.[3−5] However, the responsivity of the graphene photodetectors is limited by its atomically thin nature and the ultrafast charge carrier recombination in graphene.[6−8] One strategy to overcome this major drawback is to integrate graphene-based transistors with other light-absorbing materials such as ZnO,[9] TiO_2,[10] PbS quantum dots (QDs),[11] and organic semiconductors.[12] In these hybrid photodetectors, the conductance of graphene can be modified through electrostatic gating induced by long-lifetime photocarriers in light-absorbing materials.[11] Recently, the three-dimensional (3D) organic−inorganic halide perovskites were integrated with graphene to form hybrid phototransistors,[13] leveraging the desirable properties of 3D perovskites, such as high absorption coefficient,[14] long charge carrier diffusion length,[15] and ease in large scale fabrication.[16]

Nevertheless, the inefficient charge carrier separation process and its low resistance to moisture in these graphene−3D perovskites phototransistors lead to a relatively low photo-

Received: July 13, 2017
Revised: November 2, 2017
Published: November 7, 2017

DOI: 10.1021/acs.nanolett.7b02980
Nano Lett. 2017, 17, 7330−7338

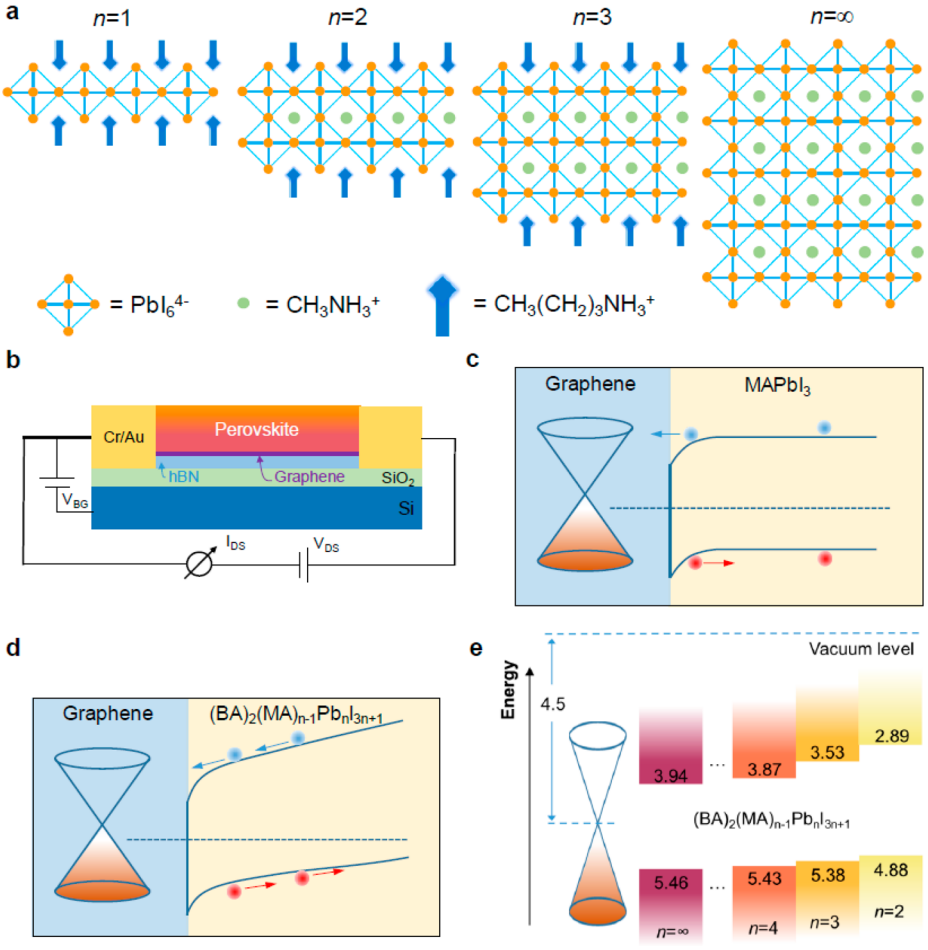

Figure 1. Operational mechanisms of the graphene−perovskite phototransistors. (a) Schematic crystal structures of $(BA)_2(MA)_{n-1}Pb_nI_{3n+1}$. (b) Schematic device structure of the graphene-perovskite phototransistor. (c) Energy level diagram of the graphene−$MAPbI_3$ phototransistor. (d) Energy level diagram of the graphene−$(BA)_2(MA)_{n-1}Pb_nI_{3n+1}$ heterostructure phototransistor, illustrating a positive sloping in the energy band for photogenerated electron−hole separation. (e) Comparative band energy diagram of the $(BA)_2(MA)_{n-1}Pb_nI_{3n+1}$ perovskites with different n. The values of VBM and CBM energies of perovskites are taken from ref 23. The intrinsic graphene work function of 4.5 eV is shown for comparison.

responsivity and short device lifetime. Lately, the two-dimensional (2D) perovskites, which consist of lead iodide octahedral layers intercalated with organic cations that act as spacers, have emerged as an alternative to 3D perovskites.[17−19] In addition to the large tunability in chemical compositions[20] and the degrees of quantum confinement,[21] the improved moisture stability[22−24] due to the wrapping of organic ligands has triggered a plethora of research interests on their optoelectronic properties and applications including their integration with graphene.[24,25]

Here, we present a graphene−2D multiphase perovskite heterostructure phototransistor based on a newly developed two-step ligand exchange spin-coating method which aligns the different 2D perovskite phases along the direction perpendicular to the substrate. The natural energy band alignment resulting from the varying 2D perovskite phases along the vertical direction facilitates the spatial separation of photogenerated charge carriers, leading to a high responsivity of $\sim 10^5$ A W^{-1} at 532 nm. In addition, compared with the 3D perovskite counterparts, the smaller $1/f$ noise measured in our graphene−2D perovskite phototransistor implies a lower density of deep traps, which results in a faster photoresponse. Furthermore, 2D perovskites prevent the permeation of moisture, a highly desirable characteristic not available in 3D perovskites. As a result, the enhanced gain, response speed, and stability have been observed in these novel graphene−2D perovskite phototransistors. Such highly sensitive phototransistors can be integrated with many different substrates including flexible ones due to the low-temperature solution processing procedures and the layered nature of all the materials involved. Moreover, the graded 2D perovskite heterostructure concept demonstrated in this work can be readily leveraged to realize high performance, air stable solar cells, and light-emitting diodes.

The 2D perovskites in this work are generally described by the formula of $(BA)_2(MA)_{n-1}Pb_nI_{3n+1}$, where $BA^+ = CH_3(CH_2)_3NH_3^+$, $MA^+ = CH_3NH_3^+$ and the integer n is the number of lead iodide octahedral layers between two BA^+ organic spacers, as shown in Figure 1a. When $n = \infty$, the material is simply the extensively studied 3D methylammonium lead iodide perovskites ($MAPbI_3$). Figure 1b shows the device structure of the graphene−2D perovskite phototransistor, which is essentially a graphene transistor covered by the 2D perovskite layer. To increase the carrier mobility in the graphene transistor, an exfoliated thin hexagonal boron nitride (hBN) flake was used underneath graphene since hBN has been shown to be an ideal substrate to preserve the intrinsically high mobility of graphene.[26] The transferred monolayer

DOI: 10.1021/acs.nanolett.7b02980
Nano Lett. 2017, 17, 7330−7338

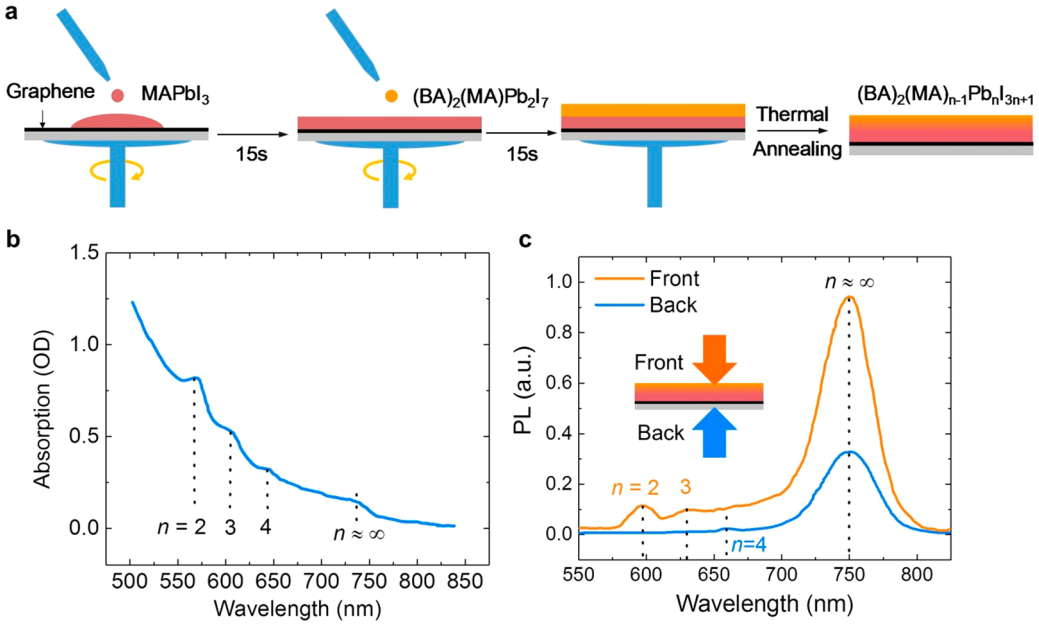

Figure 2. Fabrication and characterization of 2D perovskite heterostructure. (a) Schematic of two-cycles spin coating process for $(BA)_2(MA)_{n-1}Pb_nI_{3n+1}$ perovskite heterostructure fabrication. (b) Single-path absorption spectrum of $(BA)_2(MA)_{n-1}Pb_nI_{3n+1}$ perovskite heterostructure thin films. (c) Photoluminescence spectra of $(BA)_2(MA)_{n-1}Pb_nI_{3n+1}$ perovskite heterostructure thin films under front and back excitation with 405 nm laser.

graphene on top of the hBN flake is free of wrinkles or bubbles. The as-prepared graphene transistors exhibit room-temperature field effect mobility up to 16,000 $cm^2/(V\ s)$. The detailed material synthesis and device fabrication procedures are described in Methods. In this work, the performances of the phototransistors with both 3D perovskites $MAPbI_3$ and 2D perovskites $(BA)_2(MA)_{n-1}Pb_nI_{3n+1}$ were studied for comparison.

Figure 1c,d illustrates that an appropriate energy band alignment can promote photoexcited carrier separation and increase the gain of the graphene–perovskite phototransistors. In these devices, the perovskites act as a strong light-absorbing layer. Since the Dirac point voltage of the graphene transistor transfer curve increases after the perovskite deposition (see Figure S1), we can infer that electrons transfer from graphene to perovskites upon the contact due to their work function difference. As a result, the band bends downward at the perovskite–graphene interface as shown in Figure 1c. Thus, the photogenerated electrons can effectively transport from perovskite to graphene, while holes accumulate in the perovskite layer and lead to the photogating effect. Consequently, the sheet resistance of the graphene can be tuned through electron doping in graphene induced by accumulated holes in the perovskite layer. The photoconductive gain of the phototransistors, given by $G = \tau_{lifetime}/\tau_{transit}$, originates from the recirculation of electrons in the graphene transistor before the holes in the perovskite layer recombine. To achieve a higher gain, it is important to decrease the electron transit time $\tau_{transit}$ in the graphene transistor and increase the hole recombination lifetime $\tau_{lifetime}$ in the perovskite layer, simultaneously. At a given drain-source voltage (V_{DS}), the electron transit time is inversely proportional to the mobility of the graphene if we assume that the electric filed in the channel is low. As a result, high graphene mobility is critical for high gain in our devices. At the same time, increasing the hole recombination lifetime in perovskites requires an efficient electron–hole spatial separation scheme to reduce the probability of electron–hole annihilation. Although band bending induced built-in electric field due to the charge transfer between 3D perovskite and graphene can facilitate the separation of photogenerated electrons and holes at the interfacial region as shown in the Figure 1c, most regions in 3D perovskite have a flat band, in which the desirable electric field for charge separation does not exist. Therefore, an energy band slope across the entire perovskite layer as shown in Figure 1d is highly desirable to facilitate the charge spatial separation throughout the vertical direction of the thin film, which can increase the hole lifetime and thus the gain of the phototransistor. In fact, graded doping in 3D perovskite thin film can possibly lead to such desirable band bending but it requires challenging fabrication techniques to introduce the inhomogeneous doping across the thin film. On the other hand, the band bending can also be achieved through controlled materials composition variation. For instance, the germanium–silicon alloy with a graded bandgap has been utilized as the base in drift-field transistors for a higher current gain[27] and as the active layer in the solar cells for a higher open-circuit voltage.[28] Recent studies revealed that the spin-coated 2D perovskites thin films can consist of multiple phases with different n values.[29,30] Here, we leverage the multiple phase nature of 2D perovskites thin films to control the band bending for efficient photocarrier separation within the entire perovskite stack for high gain photodetection. It has been reported that the energy level of both the valence band maximum (VBM) and conduction band minimum (CBM) of $(BA)_2(MA)_{n-1}Pb_nI_{3n+1}$ increases with respect to decreasing n,[23] as shown in Figure 1e. For intrinsic graphene, its work function is around 4.5 eV.[31] Therefore, the desirable band bending for efficient photocarrier separation as illustrated in Figure 1d can be mimicked by varying n along the vertical direction in the multiphase perovskite heterostructure as shown in Figure 1e. The sequential distributions of 2D perovskite phases on glass in the order of n values has been reported previously.[32] Moreover,

DOI: 10.1021/acs.nanolett.7b02980
Nano Lett. 2017, 17, 7330–7338

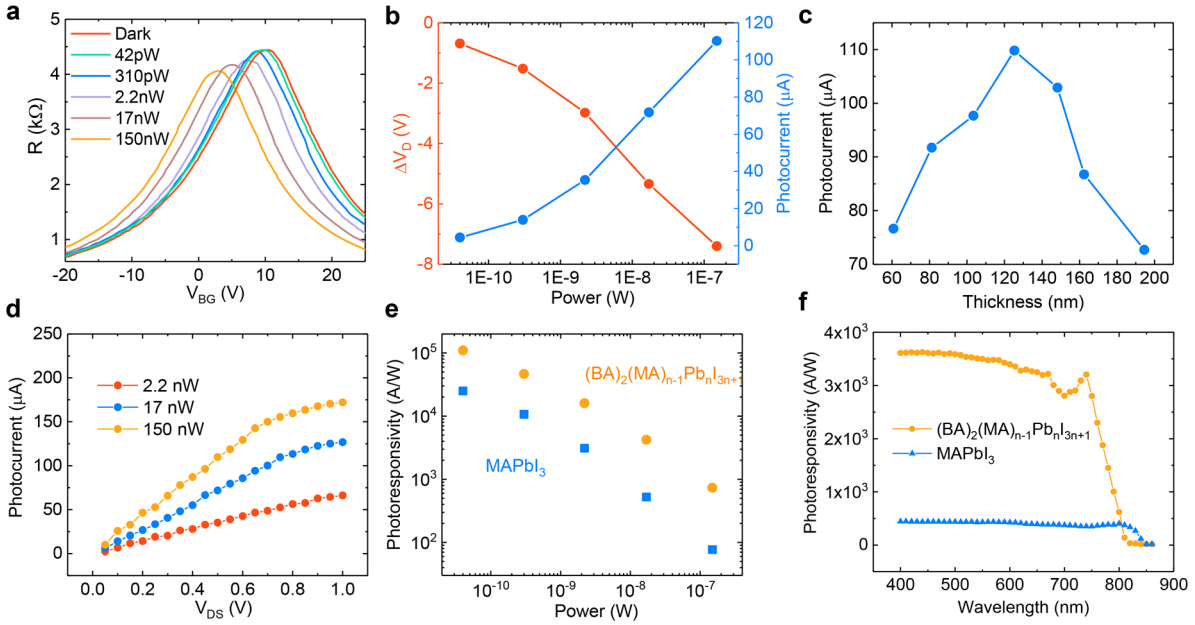

Figure 3. Characterizations of graphene−perovskite phototransistors. (a) Resistance as a function of back-gate voltage (V_{BG}) for graphene−2D perovskite heterostructure ($(BA)_2(MA)_{n-1}Pb_nI_{3n+1}$) phototransistor under different illumination powers with a drain-source voltage (V_{DS}) of 200 mV. (b) Shifts of Dirac point (ΔV_D) (left axis) and photocurrents (I_{ph}) at V_{BG} = 15 V (right axis) as a function of illumination power. The V_{DS} = 200 mV. (c) Photocurrents measured with V_{BG} = 15 V and V_{DS} = 200 mV in graphene−2D perovskite heterostructure phototransistors with different thin film thicknesses. (d) Photocurrents as a function of V_{DS} under different illumination power at V_{BG} = 15 V. (e) Photoresponsivity of phototransistor with 2D perovskite heterostructure and 3D perovskite ($MAPbI_3$) as the light absorbing material under different illumination intensities. (f) Spectra responsivity of phototransistors with 2D perovskite heterostructure and 3D perovskite as the light absorbing material measured with V_{BG} = 15 V and V_{DS} = 200 mV.

in ref 32 the carrier separation leveraging the intrinsic band bending in heterostructures was demonstrated using ultrafast optical absorption and time-resolved photoluminescence measurements. However, the small-n perovskite phases accumulate close to the bottom surface and the large-n phases accumulate close to upper surface, which is in an opposite sequence with our desirable order.

To realize the multiphase 2D perovskite heterostructure thin film with desirable n order, a two-step ligand exchange method was developed as illustrated in Figure 2a. For the first coating step, 40 μL of 100 °C preheated $MAPbI_3$ ($n = \infty$) precursor solution was dripped onto the center of the spinning substrate. After the first perovskite layer dried (~15 s), 40 μL of 100 °C preheated $(BA)_2(MA)_1PbI_7$ (n = 2) precursor solution was dripped on the spinning substrate as the second coating step. The spin coating process ended after another 15 s. The goal of using two kinds of solution with different compositions in the two-step spin coating is to induce large BA^+ concentration difference in the as-spun thin films. After spin-coating, the dried samples were annealed at 95 °C for 40 min. With the assistance of thermal energy, the organic ligands interdiffused in the $(BA)_2(MA)_{n-1}Pb_nI_{3n+1}$ perovskite thin films, generating a BA^+ concentration gradient in vertical direction. As a result, the multiple phases with different n were formed, enabling the desirable band alignment.

To examine the perovskite phase distribution in the 2D perovskite heterostructure thin films fabricated using the two-step ligand exchange spin-coating method, the absorption and photoluminescence (PL) spectroscopy experiments were carried out. The control perovskite samples used for these optical measurements were fabricated on the transparent glass substrates covered with graphene. Figure 2b shows the single-path absorption spectrum of the multiphase 2D perovskite heterostructure thin films. Four absorption peaks were observed at 569 nm (2.17 eV), 605 nm (2.04 eV), 643 nm (1.93 eV), and 735 nm (1.68 eV), respectively. Comparing with the reported absorption spectra of the 2D perovskite single crystals, the three absorption peaks at high energy can be assigned to $(BA)_2(MA)_{n-1}Pb_nI_{3n+1}$ perovskites with n = 2, 3 and 4, respectively.[32] The absorption peak with lowest energy level at 735 nm, which is close to the absorption edge of 3D $MAPbI_3$ perovskite, corresponding to a much larger n value ($n \approx \infty$). This observation reveals the hybrid nature of our 2D perovskite heterostructure thin films, which consist of multiphases with different n values. To verify whether the distribution of the different perovskite phases is in the descending order of n along the direction perpendicular to the substrate, we further conducted the PL experiments with different incident light directions. Previously, a similar technique was utilized to identify the spatial trap distributions in perovskite $MAPbI_3$ thin films.[33] The schematic of the PL measurement is shown in the inset of the Figure 2c, in which the excitation laser (405 nm) is incident either from the glass side (back excitation) or from the perovskite side (front excitation). The strong light absorption of 2D perovskites leads to a small penetration depth (≤50 nm) of the 405 nm light. Thus, the PL light excitation region is confined either close to the bottom or to the upper surface of the 2D perovskite thin films. As shown in Figure 2c, the dominant emission peak locates at 750 nm shared by both PL spectra can be attributed to the radiative charge recombination in the $n \approx \infty$ phase. For PL spectra with the front excitation, additional emission peaks corresponding to n = 2, 3 were observed. On the contrary, the emission peak corresponding to n = 4 was observed in PL spectra under back excitation. Considering the small penetration depth of the 405 nm light, the results indicate that 2D perovskite phases with small n

DOI: 10.1021/acs.nanolett.7b02980
Nano Lett. 2017, 17, 7330−7338

locate close to the upper surface while the large n perovskite phases mainly accumulate close to the bottom of the thin films. Such phase distribution forms a graded heterostructure desirable for a high-gain photodetection as discussed above. Here we want to emphasize that the absorption spectrum shown in Figure 2b is similar to that reported in ref 32, since the absorption does not depend on the alignment direction of the perovskite heterostructures. However, the photoluminescence spectrum with front excitation in this work (Figure 2c) is similar to that with back excitation in ref 32 and vice versa due to the different perovskite phase alignment direction.

On the basis of such 2D perovskite heterostructure thin films with optimized energy band bending, high-gain graphene−2D perovskite heterostructure phototransistors were fabricated. The width and length of the graphene channel are 2 and 8 μm, respectively. Optical micrographs of the graphene phototransistor before and after 2D perovskite heterostructure deposition are shown in Figure S1. Figure 3a shows a typical result of the resistance as a function of back-gate voltage (V_{BG}) under different optical excitation powers at a fixed drain-source voltage V_{DS} of 200 mV. The devices show negligible hysteresis with different scanning directions no matter in dark or illumination conditions (see Figure S2). As the light intensity increases, the Dirac point V_D, where the device resistance reaches its maximum, shifts toward a lower V_{BG}, implying an electron doping of the graphene channel induced by the light. In our phototransistors, incident light generates electron−hole pairs in 2D perovskite heterostructure, which are dissociated effectively by the built-in band bending. The electrons transport to graphene, and the holes accumulate in 2D perovskite heterostructure thin films. The photogating effect, induced by the accumulated holes in perovskites, produces an electron current in the graphene through capacitive coupling and shifts the Dirac point voltage of graphene transistor (V_D) to lower back gate bias (V_{BG}). Furthermore, when $V_{BG} < V_D$, the carriers traveling in the graphene channel is hole-dominant, which can recombine with the electrons transport from perovskite to graphene and the electrons induced by photogating effect. Thus, the increasing light intensity would increase the resistance. In contrast, when $V_{BG} > V_D$, electron is the dominant charge carrier in the graphene and thus the photogating effect leads to a decrease of resistance. Shifts of V_D and the photocurrents ($I_{ph} = I_{light} - I_{dark}$) measured at V_{BG} = 15 V were summarized in Figure 3b. More holes accumulated in the 2D perovskites as the illumination intensity increases, inducing stronger photogating effect and larger photocurrents.

The dependence of photocurrent on 2D perovskite thin film thickness was studied as shown in Figure 3c. All photocurrents were measured with V_{BG} = 15 V and V_{DS} = 200 mV. The thickness of 2D perovskite layer was varied from 60 to 194 nm by tuning the concentration of $MAPbI_3$ and $(BA)_2(MA)PbI_7$ precursor solutions and the spin-coating rate. The photocurrents first increase and then decrease as the 2D perovskite thin film thickness increase. The maximum photocurrent was obtained in devices with 125 nm-thick 2D perovskite thin film. For devices with 2D perovskite thinner than 125 nm, the reduced absorption of the incident light results in the photocurrent decrease. On the other hand, the thicker 2D perovskite thin films tend to attenuate the capacitive coupling effect as the photoexcited holes accumulate close to the upper surface of the 2D perovskite layer, leading to reduced photoresponse.

Figure 3d shows the dependence of photocurrent on source-drain bias V_{DS} measured at V_{BG} = 15 V. For a given light intensity, the I_{ph} first increase linearly with V_{DS} and then gradually saturate at high V_{DS} bias. In addition, the source-drain voltage V_{DS} at which the photocurrent I_{ph} starts to saturate decreases as the light power increases. The photocurrent saturation effect could be attributed to the ion migrations in perovskites,[34] which tends to screen the external electric fields.[35] Previous studies show that the electric fields about 0.3 V/μm could drive MA^+ ions to migrate in $MAPbI_3$ 3D perovskites in dark.[36] Here, the ions readily migrate at a smaller electric field (~0.1 V/μm under 150 nW light illumination) with the assistance of incident light. Thus, to protect the samples from irreversible damage,[34] the V_{DS} bias keeps at 200 mV for all the other measurements in this study.

The photoresponsivity of our devices, defined as $R = I_{ph}/P$, was summarized in Figure 3d. The inverse relation between R and P can be attributed to that the built-in electric field in perovskite was weakened by the increasing number of photogenerated holes under higher light illumination.[11] At an incident light power of 42 pW, a high photoresponsivity of ~10^5 A/W is observed. The photoresponsivity is comparable or higher than that of reported 3D perovskites light-absorbing layer (Figure S3) at a similar excitation light intensity.[9] We also investigated the wavelength-dependent responsivity by measuring the external quantum efficiency (EQE) of the graphene−2D perovskite phototransistors with V_{BG} = 15 V and V_{DS} = 200 mV. The spectra responsivity is given by $R = e \times \lambda \times EQE/(hc)$, where e is the elementary charge, λ is the excitation wavelength, h is Planck's constant, and c is the light velocity. As shown in Figure 3f, the strong responsivity is observed in a broad wavelength range from 400 to 740 nm, and this observation is consistent with the absorption spectra of the 2D perovskite thin films.

We also fabricated and characterized the control devices with 3D perovskites ($MAPbI_3$) as photoactive layer based on the same processes as those in the high efficiency perovskite solar cells.[37] In these devices, the 3D perovskite layer has the same thickness (~125 nm) as the 2D counterparts. This thickness in fact leads to almost complete absorption of light in the wavelength range from 400 to 740 nm for both 2D and 3D perovskites. As shown in Figure 3d,e, the graphene−2D perovskite phototransistors are superior to the 3D counterparts in terms of both power- and wavelength-dependent photoresponsivity. The enhancement in photoresponsivity by 1 order of magnitude demonstrates the effectiveness of our strategy. The effective spatial separation of the photogenerated electrons and holes facilitated by the internal band bending in 2D perovskite heterostructure thin films indeed prolongs the lifetime of the photoexcited holes and improve the photosensitivity of the phototransistor.

Another important parameter of phototransistors is the response speed. The temporal photoresponse of the phototransistors with 2D and 3D perovskite thin films were characterized using a laser pulse at 532 nm. Figure 4a,b shows the transient photocurrent measured at V_{DS} = 200 mV at an incident light power of 150 nW for 2D and 3D perovskite phototransistors, respectively. The ON-OFF switching behavior is robust and reproducible for multiple cycles (Figure S4). For graphene−2D perovskite phototransistors, the decay of the photocurrents after switching off the laser pulse has a fast component of 14.8 ms and a slow component of 175 ms, indicating the existence of different charge recombination

DOI: 10.1021/acs.nanolett.7b02980
Nano Lett. 2017, 17, 7330−7338

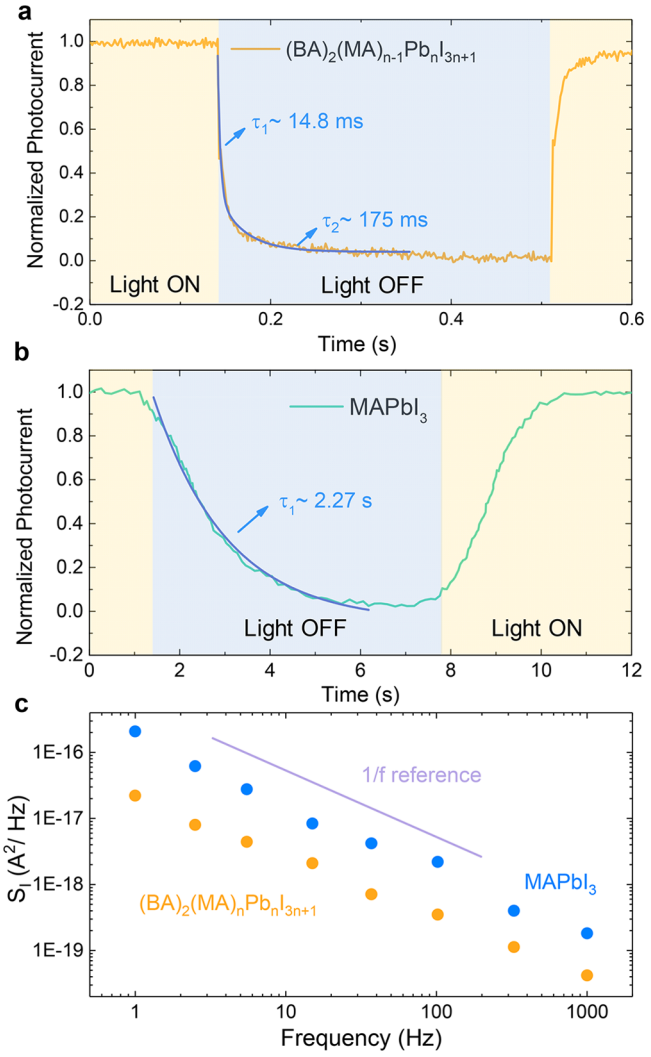

Figure 4. Temporal photocurrent response and low frequency noise measurement of the graphene–perovskite phototransistors. (a,b) Temporal photocurrent response of the phototransistors with 2D perovskite heterostructure and 3D perovskite as the light absorbing material. (c) Current noise power spectral density of the phototransistors with 2D perovskite heterostructure and 3D perovskite as the light absorbing material.

pathways for holes in the 2D perovskite layer. The multiple-exponential decay time can be attributed to hole traps with different trap depths since deeper traps in perovskites have longer charge release times and thus result in a slower photoresponse speed. The result is consistent with the mixed nature of the multiphased 2D perovskite thin films. Although the temporal photoresponse is slower than that of reported perovskite photodiodes,[38,39] the photoresponse speed of 2D perovskite phototransistor is much faster than its 3D counterpart. The decay process has only one long time constant of 2.27 s for 3D perovskite phototransistor, implying that the traps in 3D perovskites locate deeper in energetic profiles than those in 2D perovskites. The results agree with the observations in the reported 2D–3D hybrid perovskite light-emitting diodes that the density of deep traps decreases as the ratio of 2D perovskites increases.[40] Calculations also predict that the deep traps in 2D perovskites are difficult to formed or could be easily converted to inactive sites.[41]

To determine the sensitivity of graphene–perovskite phototransistors, the total current noise power spectral density (S_I), including shot noise, thermal noise and $1/f$ noise was measured in dark at low frequency (1 to 1000 Hz) with V_{BG} = 15 V and V_{DS} = 200 mV using a low noise current amplifier together with a lock-in amplifier. As shown in Figure 4c, the $1/f$ noise, which may originate from the trapping and detrapping process of large numbers of charges, dominates the low frequency noise in phototransistor with both 3D and 2D perovskite as the light absorbing material. The $1/f$ noise in the graphene–3D perovskite phototransistor is about 1 order of magnitude higher than that in the 2D counterparts, which again confirms the larger density of deep traps in 3D perovskites. On the basis of the measured noise, the specific detectivity D^* can be calculated by the following expression:[42] $D^* = (AB)^{1/2} \times R/\delta i$, where A is the effective device area, B is the bandwidth, R is the photoresponsivity, and δi is the noise current density which equates to square root of S_I at low frequency. Under incident light power of 42 pW, this yields specific detectivity D^* of 3.3×10^{10} and 9.4×10^8 Jones for phototransistors with 2D and 3D perovskites, respectively.

Finally, the stability of our phototransistors was investigated. It has been widely reported that the 3D perovskite-based optoelectronic devices suffer from a short lifetime due to its low resistance to moisture. As shown in Figure 5a, the phototransistors with 3D perovskites degrade in air quickly. Its

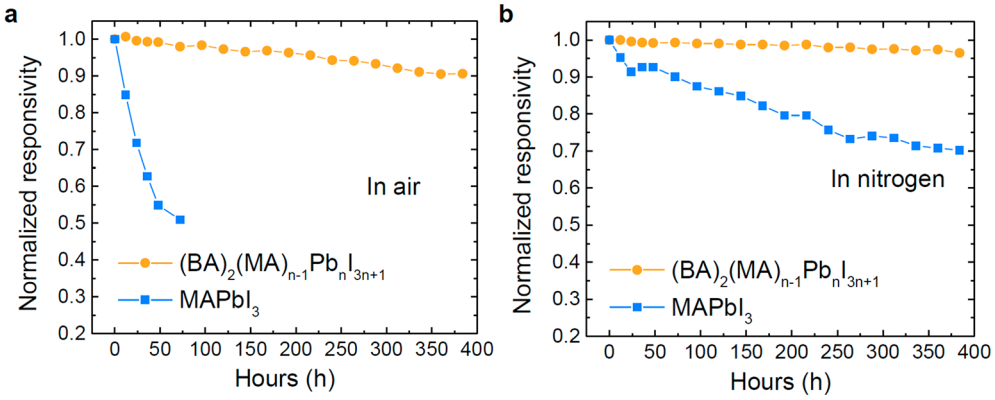

Figure 5. Stability measurements of the graphene–perovskite phototransistors. (a) Responsivity as a function of time for the phototransistors stored in air with 2D perovskite heterostructure and 3D perovskite as the light absorbing material. (b) Responsivity as a function of time for the phototransistors in dry nitrogen with 2D perovskite heterostructure and 3D perovskite as the light absorbing material.

DOI: 10.1021/acs.nanolett.7b02980
Nano Lett. 2017, 17, 7330–7338

photoresponse reduces to around 50% of its original value after exposing in air for 72 h. The $MAPbI_3$ layer decomposed to PbI_2 as the color of the thin films changed from black to yellow. On the contrary, being wrapped with organic ligands, the 2D counterparts with small n has been demonstrated theoretically and experimentally with significantly enhanced moisture stability.[17−19] Here, the 2D perovskite phases with small n close to the upper surface act as an encapsulation layer which blocks the permeation of moisture. As a result, the devices with 2D perovskites have an outstanding stability performance: the photoresponse retained 90% of its original value after more than 400 h in air without any encapsulation. For devices with 2D and 3D perovskites stored in nitrogen environment, the responsivity retain 96% and 70% of its original values after more than 400 h, respectively, as shown in Figure 5b.

In summary, we introduced a two-cycle spin-coating method to align the 2D perovskite phases along the direction perpendicular to substrate in the order of n. The formed built-in electric field in such 2D perovskite heterostructures with energy band bending facilitates the electron−hole spatial separation, which enhances the gain of the graphene−perovskite phototransistors. In addition, the graphene−2D perovskite phototransistors have a faster photoresponse speed than that of the 3D counterparts, benefiting from the relatively shallow traps. Furthermore, the stability of the devices dramatically improves in 2D perovskite devices due to the encapsulation function of the 2D perovskite phases with small n close to the upper surface. All three improvements in our phototransistors can also be leveraged to enhance the performance of 2D perovskite heterostructure solar cells. First, the internal charge separation demonstrated in our study can facilitate the exciton dissociation in 2D perovskite heterostructure solar cells. Second, the low density of deep traps reduces the trap-assistant recombination in 2D perovskite solar cells and underpins a high efficiency. At last, the improved moisture stability from the intrinsic property of 2D perovskites is ideal for photovoltaic application. As discussed above, a previous work[32] leveraging hot-casting process also realized the sequential distributions of 2D perovskite phases on glass in the order of n values but in an opposite sequence with our results. The opposite order may arise from the different fabrication process and the different hydrophobicity between the graphene and glass substrate. These two methods can be used complementarily in the fabrications of 2D perovskite solar cells with p-i-n and n-i-p structures.

Methods. *Perovskite Precursor Synthesis.* For BAI synthesis, the aqueous solution of n-Butylamine (BA, $CH_3(CH_2)_3NH_2$) (20 mL, 99.5%, Sigma-Aldrich) was mixed with hydroiodic acid (HI) (15 mL, 40 wt % in aqueous solution, Alfa Aesar) at 0 °C for 3 h in nitrogen environment. The generated mixture of clear solution was put inside a rotary evaporator to remove the solvent and form the crystallized white powder. The powder was then washed with mixture of diethyl ether (Alfa Aesar) and ethanol (Sigma-Aldrich) twice and kept dried in vacuum at room temperature. MAI was synthesized with the same method as BAI, except for the solution used. Here, 13.5 mL (40 wt % in aqueous solution; Alfa Aesar) methylamine (CH_3NH_2) was mixed with HI for MAI synthesis.

Device Fabrication. The fabrication of bottom graphene transistor started with the mechanical exfoliated hexagonal boron nitride (hBN) flakes (30−40 nm thick) on a silicon wafer with 90 nm of silicon oxide (SiO_2). The exfoliated monolayer graphene was transferred on top of the hBN by the dry transfer method as reported previously.[43] The stacked hBN/graphene layers were then annealed at 600 °C for 6 h. Afterward, the poly(methyl methacrylate) (PMMA) resist was spun on the whole wafer and patterned using a Vistec 100 kV electron-beam lithography system for metallization. Chromium/Gold (3/30 nm) were then thermally evaporated in sequential order and the following lift-off process in acetone defined the source, drain, and voltage probe contacts. After the fabrication of the bottom graphene transistor, a two-step spin coating method was conducted to fabricate the 2D perovskite layer on top of the graphene transistor. Before spin coating, solution 1 was prepared by dissolving CH_3NH_3I and PbI_2 with a molar ratio of 1:1 in *N*,*N*-dimethylformamide (DMF) and solution 2 was prepared by dissolving $CH_3(CH_2)_3NH_3I$, CH_3NH_3I, and PbI_2 with a molar ratio of 2:1:2 in *N*,*N*-DMF. The total Pb^{2+} molar concentration is 0.15 M in both solutions 1 and 2. For the first step, 40 μL of preheated solution 1 at 100 °C was spun on the wafer at 6000 r.p.m. After 15 s, without stopping the spin-coating process 40 μL of preheated solution 2 at 100 °C was dropped on the wafer as the second step. After another 15 s of spin-coating, the as-prepared device was thermal annealed at 95 °C for 40 min. The fabrication procedures for $MAPbI_3$ layer are the same as those reported in previous studies.[37]

Film and Device Characterization. The absorption spectrum (single-pass) was measured in an Evolution 201 UV−vis spectrometer. The PL spectrum was acquired by iHR320 Photoluminescence Spectroscopy. EQE measurement was done in a Newport QE measurement kit. All the other photoresponse characterizations were conducted using an Agilent B1500A semiconductor parameter analyzer together with a homemade setup. A 532 nm green laser beam was focused on the sample using a long working distance 20× microscope objective. The incident light intensity was controlled by a neutral filter and recorded by a power meter (Thorlabs PM100D). All measurements were performed in air except noise measurement, which were conducted in vacuum in a Lakeshore probe station with micromanipulation probes. The current noise was amplified by low noise current amplifier DLPCA-200 and recorded with SR830 lock-in amplifier in dark at room temperature.

■ ASSOCIATED CONTENT

Supporting Information

The Supporting Information is available free of charge on the ACS Publications website at DOI: 10.1021/acs.nanolett.7b02980.

Experimental details on the graphene transistors before and after 2D perovskite heterostructure deposition, resistance as a function of back-gate voltage (V_{BG}) of the graphene−2D perovskite phototransistor, comparison of responsivity of different graphene−perovskite phototransistors and the temporal photoresponse of the phototransistors with 2D perovskite heterostructure and 3D perovskite thin films (PDF)

■ AUTHOR INFORMATION

Corresponding Authors

*E-mail: fengnian.xia@yale.edu.
*E-mail: jhuang2@unl.edu.

DOI: 10.1021/acs.nanolett.7b02980
Nano Lett. 2017, 17, 7330−7338

ORCID

Jaemin Kong: 0000-0002-6496-9879
Kenji Watanabe: 0000-0003-3701-8119
Jinsong Huang: 0000-0002-0509-8778
Fengnian Xia: 0000-0001-5176-368X

Present Address

[⊥](I.S.) Center for Integrated Nanotechnologies, Materials Physics and Applications Division, Los Alamos National Laboratory, Los Alamos, New Mexico 87545.

Author Contributions

The manuscript was written through contributions of all authors. All authors have given approval to the final version of the manuscript.

Notes

The authors declare no competing financial interest.

■ ACKNOWLEDGMENTS

We thank Sonya Sawtelle and Professor Mark A. Reed at Department of Electrical Engineering of Yale University for help with wire bonding. F.X. acknowledges the support from the Air Force Office of Scientific Research (FA9550-14-1-0277) and the Office of Naval Research (N00014-14-0565). Facilities use in Yale was partially supported by Yale Institute for Nanoscience and Quantum Engineering (YINQE) and NSF MRSEC DMR 1119826. J.H. thanks financial support from National Science Foundation under award CMMI-1265834 and Department of Home Security award 2014-DN-077-ARI069-03. K.W. and T.T. acknowledge support from the Elemental Strategy Initiative conducted by the MEXT, Japan and JSPS KAKENHI Grant JP15K21722.

■ REFERENCES

(1) Novoselov, K. S.; Geim, A. K.; Morozov, S. V.; Jiang, D.; Zhang, Y.; Dubonos, S. V.; Grigorieva, I. V.; Firsov, A. A. *Science* **2004**, *306*, 666−669.

(2) Nair, R. R.; Blake, P.; Grigorenko, A. N.; Novoselov, K. S.; Booth, T. J.; Stauber, T.; Peres, N. M.; Geim, A. K. *Science* **2008**, *320*, 1308−1308.

(3) Pospischil, A.; Humer, M.; Furchi, M. M.; Bachmann, D.; Guider, R.; Fromherz, T.; Mueller, T. *Nat. Photonics* **2013**, *7*, 892−896.

(4) Wang, X.; Cheng, Z.; Xu, K.; Tsang, H. K.; Xu, J.-B. *Nat. Photonics* **2013**, *7*, 888−891.

(5) Gan, X.; Shiue, R.-J.; Gao, Y.; Meric, I.; Heinz, T. F.; Shepard, K.; Hone, J.; Assefa, S.; Englund, D. *Nat. Photonics* **2013**, *7*, 883−887.

(6) George, P. A.; Strait, J.; Dawlaty, J.; Shivaraman, S.; Chandrashekhar, M.; Rana, F.; Spencer, M. G. *Nano Lett.* **2008**, *8*, 4248−4251.

(7) Dawlaty, J. M.; Shivaraman, S.; Strait, J.; George, P.; Chandrashekhar, M.; Rana, F.; Spencer, M. G.; Veksler, D.; Chen, Y. *Appl. Phys. Lett.* **2008**, *93*, 131905.

(8) Mueller, T.; Xia, F.; Avouris, P. *Nat. Photonics* **2010**, *4*, 297−301.

(9) Guo, W.; Xu, S.; Wu, Z.; Wang, N.; Loy, M.; Du, S. *Small* **2013**, *9*, 3031−3036.

(10) Manga, K. K.; Wang, S.; Jaiswal, M.; Bao, Q.; Loh, K. P. *Adv. Mater.* **2010**, *22*, 5265−5270.

(11) Konstantatos, G.; Badioli, M.; Gaudreau, L.; Osmond, J.; Bernechea, M.; De Arquer, F. P. G.; Gatti, F.; Koppens, F. H. *Nat. Nanotechnol.* **2012**, *7*, 363−368.

(12) Liu, X.; Luo, X.; Nan, H.; Guo, H.; Wang, P.; Zhang, L.; Zhou, M.; Yang, Z.; Shi, Y.; Hu, W. *Adv. Mater.* **2016**, *28*, 5200−5205.

(13) Lee, Y.; Kwon, J.; Hwang, E.; Ra, C. H.; Yoo, W. J.; Ahn, J. H.; Park, J. H.; Cho, J. H. *Adv. Mater.* **2015**, *27*, 41−46.

(14) Xiao, Z.; Dong, Q.; Bi, C.; Shao, Y.; Yuan, Y.; Huang, J. *Adv. Mater.* **2014**, *26*, 6503−6509.

(15) Dong, Q.; Fang, Y.; Shao, Y.; Mulligan, P.; Qiu, J.; Cao, L.; Huang, J. *Science* **2015**, *347*, 967−970.

(16) Moore, D. T.; Sai, H.; Tan, K. W.; Smilgies, D.-M.; Zhang, W.; Snaith, H. J.; Wiesner, U.; Estroff, L. A. *J. Am. Chem. Soc.* **2015**, *137*, 2350−2358.

(17) Dou, L.; Wong, A. B.; Yu, Y.; Lai, M.; Kornienko, N.; Eaton, S. W.; Fu, A.; Bischak, C. G.; Ma, J.; Ding, T. *Science* **2015**, *349*, 1518−1521.

(18) Stoumpos, C. C.; Cao, D. H.; Clark, D. J.; Young, J.; Rondinelli, J. M.; Jang, J. I.; Hupp, J. T.; Kanatzidis, M. G. *Chem. Mater.* **2016**, *28*, 2852−2867.

(19) Milot, R. L.; Sutton, R. J.; Eperon, G. E.; Haghighirad, A. A.; Martinez Hardigree, J.; Miranda, L.; Snaith, H. J.; Johnston, M. B.; Herz, L. M. *Nano Lett.* **2016**, *16*, 7001−7007.

(20) Quan, L. N.; Yuan, M.; Comin, R.; Voznyy, O.; Beauregard, E. M.; Hoogland, S.; Buin, A.; Kirmani, A. R.; Zhao, K.; Amassian, A. *J. Am. Chem. Soc.* **2016**, *138*, 2649−2655.

(21) Giovanni, D.; Chong, W. K.; Dewi, H. A.; Thirumal, K.; Neogi, I.; Ramesh, R.; Mhaisalkar, S.; Mathews, N.; Sum, T. C. *Sci. Adv.* **2016**, *2*, e1600477.

(22) Smith, I. C.; Hoke, E. T.; Solis-Ibarra, D.; McGehee, M. D.; Karunadasa, H. I. *Angew. Chem.* **2014**, *126*, 11414−11417.

(23) Cao, D. H.; Stoumpos, C. C.; Farha, O. K.; Hupp, J. T.; Kanatzidis, M. G. *J. Am. Chem. Soc.* **2015**, *137*, 7843−7850.

(24) Tsai, H.; Nie, W.; Blancon, J.-C.; Stoumpos, C. C.; Asadpour, R.; Harutyunyan, B.; Neukirch, A. J.; Verduzco, R.; Crochet, J. J.; Tretiak, S. *Nature* **2016**, *536*, 312−316.

(25) Tan, Z.; Wu, Y.; Hong, H.; Yin, J.; Zhang, J.; Lin, L.; Wang, M.; Sun, X.; Sun, L.; Huang, Y.; Liu, K.; Liu, Z.; Peng, H. *J. Am. Chem. Soc.* **2016**, *138*, 16612−16615.

(26) Dean, C. R.; Young, A. F.; Meric, I.; Lee, C.; Wang, L.; Sorgenfrei, S.; Watanabe, K.; Taniguchi, T.; Kim, P.; Shepard, K. L.; et al. *Nat. Nanotechnol.* **2010**, *5*, 722−726.

(27) Kroemer, H. *Rca Rev.* **1957**, *18*, 332−342.

(28) Pham, D. P.; Kim, S.; Park, J.; Le, A. T.; Cho, J.; Jung, J.; Iftiquar, S.; Yi, J. *Mater. Sci. Semicond. Process.* **2016**, *56*, 183−188.

(29) Wang, N.; Cheng, L.; Ge, R.; Zhang, S.; Miao, Y.; Zou, W.; Yi, C.; Sun, Y.; Cao, Y.; Yang, R.; Wei, Y.; Guo, Q.; Ke, Y.; Yu, M.; Jin, Y.; Liu, Y.; Ding, Q.; Di, D.; Yang, L.; Xing, G.; Tian, H.; Jin, C.; Gao, F.; Friend, R. H.; Wang, J.; Huang, W. *Nat. Photonics* **2016**, *10*, 699−704.

(30) Yuan, M.; Quan, L. N.; Comin, R.; Walters, G.; Sabatini, R.; Voznyy, O.; Hoogland, S.; Zhao, Y.; Beauregard, E. M.; Kanjanaboos, P.; Lu, Z.; Kim, D. H.; Sargent, E. H. *Nat. Nanotechnol.* **2016**, *11*, 872−877.

(31) Yu, Y.-J.; Zhao, Y.; Ryu, S.; Brus, L. E.; Kim, K. S.; Kim, P. *Nano Lett.* **2009**, *9*, 3430−3434.

(32) Liu, J.; Leng, J.; Wu, K.; Zhang, J.; Jin, S. *J. Am. Chem. Soc.* **2017**, *139*, 1432−1435.

(33) Shao, Y.; Xiao, Z.; Bi, C.; Yuan, Y.; Huang, J. *Nat. Commun.* **2014**, *5*, 5784.

(34) Xiao, Z.; Yuan, Y.; Shao, Y.; Wang, Q.; Dong, Q.; Bi, C.; Sharma, P.; Gruverman, A.; Huang, J. *Nat. Mater.* **2014**, *14*, 193−198.

(35) Chin, X. Y.; Cortecchia, D.; Yin, J.; Bruno, A.; Soci, C. *Nat. Commun.* **2015**, *6*, 7383.

(36) Yuan, Y.; Chae, J.; Shao, Y.; Wang, Q.; Xiao, Z.; Centrone, A.; Huang, J. *Adv. Energy Mater.* **2015**, *5*, 1500615.

(37) Wang, Q.; Shao, Y.; Dong, Q.; Xiao, Z.; Yuan, Y.; Huang, J. *Energy Environ. Sci.* **2014**, *7*, 2359−2365.

(38) Deng, H.; Yang, X.; Dong, D.; Li, B.; Yang, D.; Yuan, S.; Qiao, K.; Cheng, Y.-B.; Tang, J.; Song, H. *Nano Lett.* **2015**, *15*, 7963−7969.

(39) Dou, L.; Yang, Y. M.; You, J.; Hong, Z.; Chang, W.-H.; Li, G.; Yang, Y. *Nat. Commun.* **2014**, *5*, 5404.

(40) Byun, J.; Cho, H.; Wolf, C.; Jang, M.; Sadhanala, A.; Friend, R. H.; Yang, H.; Lee, T. W. *Adv. Mater.* **2016**, *28*, 7515−7520.

(41) Liu, Y.; Xiao, H.; Goddard, W. A., III *Nano Lett.* **2016**, *16*, 3335−3340.

(42) Gong, X.; Tong, M.; Xia, Y.; Cai, W.; Moon, J. S.; Cao, Y.; Yu, G.; Shieh, C.-L.; Nilsson, B.; Heeger, A. J. *Science* **2009**, *325*, 1665−1667.

DOI: 10.1021/acs.nanolett.7b02980
Nano Lett. 2017, 17, 7330−7338

(43) Leon, J.; Mamani, N.; Rahim, A.; Gomez, L.; da Silva, M.; Gusev, G. *Graphene* **2014**, *03*, 25−35.

DOI: 10.1021/acs.nanolett.7b02980
Nano Lett. 2017, 17, 7330−7338